Spatial distribution of the emission intensity in a photonic crystal: Self-interference of Bloch eigenwaves

Dmitry N. Chigrin*
Physikalisches Institut, Universität Bonn, Nussallee 12, D-53115 Bonn, Germany

The analysis of an angular distribution of the emission intensity of a two-level atom (dipole) in a photonic crystal reveals an enhancement of the emission rate in some observation directions. Such an enhancement is the result of the bunching of many Bloch eigenwaves with different wave vectors in the same direction due to the crystal anisotropy. If a spatial distribution of the emission intensity is considered, the interference of these eigenwaves should be taken into account. In this paper, the far-field emission pattern of a two-level atom is discussed in the framework of the asymptotic analysis the classical macroscopic Green function. Numerical example is given for a two-dimensional square lattice of air holes in polymer. The relevance of results for experimental observation is discussed.

PACS numbers: 42.70.Qs; 42.25.Fx; 42.50.Pq; 81.05.Zx

I. INTRODUCTION

Light emission in a photonic crystal has attracted a substantial attention both in theoretical [1, 2, 3, 4, 5, 6, 7, 8, 9, 10, 11, 12] and experimental [13, 14, 15, 16, 17, 18, 19, 20, 21, 22] studies. To a large extend this interest is due to potential perspectives of the emission modification and control provided by photonic crystals. The inhibition of spontaneous emission is possible within a spectral range of a complete photonic bandgap [1, 2], where linear propagation of light is prohibited in all spatial directions. An emission enhancement is a result of a long interaction time of an emitter and the radiated field, when the emitter is coupled to the slow eigenmode [7, 13, 23] or to the strongly localized mode of a defect state of a photonic crystal [24, 25, 26].

It is well known that, the spontaneous decay of an excited atom strongly depends on the environment [27]. Both the emission rate and the emission directionality can be affected. In the simplest case of a two-level atom placed in an inhomogeneous medium the emission dynamics can be described by the integro-differential equation for the upper state occupation probability amplitude [8, 28]

$$\dot{C}(t) = -\int_0^t dt' \, K(t-t') \, C(t) \tag{1}$$

with the kernel $K(t-t')$defined by

$$K(t-t') = \frac{1}{2\hbar\varepsilon_0} \int_0^\infty d\omega \, \omega \rho(\mathbf{r}_0, \omega) \, e^{-i(\omega-\omega_0)(t-t')}, \tag{2}$$

where

$$\rho(\mathbf{r}_0, \omega) = \frac{2\omega}{\pi c^2} \mathbf{d} \cdot \mathrm{Im}\left[\overleftrightarrow{\mathbf{G}}(\mathbf{r}_0, \mathbf{r}_0, \omega)\right] \cdot \mathbf{d} \tag{3}$$

is the projected local density of states (PLDOS) [29, 30]. $\overleftrightarrow{\mathbf{G}}(\mathbf{r}, \mathbf{r}', \omega)$ is the classical macroscopic dyadic Green function defined by the inhomogeneous wave equation [31]

$$\left(\frac{\omega^2}{c^2}\varepsilon(\mathbf{r}) - \nabla \times \nabla \times\right) \overleftrightarrow{\mathbf{G}}(\mathbf{r}, \mathbf{r}', \omega) = -\overleftrightarrow{\delta}_{\epsilon_\perp}(\mathbf{r} - \mathbf{r}'). \tag{4}$$

Here $\overleftrightarrow{\delta}_{\epsilon_\perp}(\mathbf{r} - \mathbf{r}')$ is the ε-transverse dyadic delta function [4, 32], $\mathbf{r}_0$, ω_0 and $\mathbf{d}$ are atom location, transition frequency and transition dipole moment, respectively. c is a speed of light in vacuum. In the case of a general linear, non-magnetic, dielectric medium with arbitrary three-dimensional (3D) periodic dielectric function, $\varepsilon(\mathbf{r})$, the Green's function can be expressed in the Bloch mode basis as [4, 31]

$$\overleftrightarrow{\mathbf{G}}(\mathbf{r}, \mathbf{r}', \omega) = \frac{c^2}{V} \sum_{n\mathbf{k}} \frac{\mathbf{A}_{n\mathbf{k}}(\mathbf{r}) \otimes \mathbf{A}^*_{n\mathbf{k}}(\mathbf{r}')}{\omega^2_{n\mathbf{k}} - (\omega + i\gamma)^2} \tag{5}$$

Here $\mathbf{A}_{n\mathbf{k}}(\mathbf{r})$ are Bloch eigenwaves characterized by the band index n, the wave vector $\mathbf{k}_n$ and the eigenfrequencies $\omega_{n\mathbf{k}}$. Bloch eigenwaves are solutions of the homogeneous wave equation and obey the gauge $\nabla \cdot [\varepsilon(\mathbf{r})\mathbf{A}_{n\mathbf{k}}(\mathbf{r})] = 0$, normalization and completeness conditions [4, 32]. The asterisk $*$ and $\otimes$ denote the complex conjugate and the outer tensor product, respectively. A positive infinitesimal γ assures causality.

In the limit of the weak coupling (Markov approximation), a coarse-grained description of the atomic motion memory effects can be disregarded [8, 28] and Eq. (1) yields the familiar exponential decay of the excited state with a decay rate given by

$$\begin{aligned} \Gamma(\omega_0) &= \frac{\pi\omega_0}{\hbar\varepsilon_0} \rho(\mathbf{r}_0, \omega_0) \\ &= \frac{\pi\omega_0}{\hbar\varepsilon_0 V} \sum_{n\mathbf{k}} |\mathbf{A}_{n\mathbf{k}}(\mathbf{r}_0) \cdot \mathbf{d}|^2 \, \delta(\omega_0 - \omega_{n\mathbf{k}}) \end{aligned} \tag{6}$$

and the spatial distribution of the emitted intensity given

*Electronic address: chigrin@th.physik.uni-bonn.de

by [28]

$$I(\mathbf{r},\omega_0) = \left|\frac{\omega_0^2}{\varepsilon_0 c^2}\overleftrightarrow{\mathbf{G}}(\mathbf{r},\mathbf{r}_0,\omega_0)\cdot\mathbf{d}\right|^2 = \left|\frac{\omega_0^2}{\varepsilon_0 V}\sum_{n\mathbf{k}}\frac{(\mathbf{A}^*_{n\mathbf{k}}(\mathbf{r}_0)\cdot\mathbf{d})\,\mathbf{A}_{n\mathbf{k}}(\mathbf{r})}{\omega^2_{n\mathbf{k}}-(\omega_0+i\gamma)^2}\right|^2. \quad (7)$$

This approximation gives the correct result for emission modification in most of the situations considered in the present paper. In the same time, special care should be taken for frequencies near the photonic band edges or other van Hove singularities, where the memory effects become significant and Eq. (1) should be analyzed instead of a direct use of Eqs. (6,7).

In Eqs. (1) and (6,7) all parameters of a periodic environment relevant for the atomic evolution are contained via the classical Green function and its Bloch mode expansion (5). The emission rate (6) is proportional to the density of available Bloch eigenmodes weighed by the coupling strength between the atomic dipole moment and the corresponding mode. The emitted intensity (7) at the point $\mathbf{r}$ is determined both by the spectral and angular emission rate modification and by the interference of the Bloch modes at this point.

In contrast to the total emission rate modification (6), angular-resolved emission experiments, e.g. [21, 22], usually probe only a small fraction of the solid angle detecting the emission modification in a particular direction in space. To analyzed such angular-resolved emission experiments, a fractional power emitted per solid angle in space can introduced. It has been shown, that the radiation pattern of the classical dipole in a photonic crystal can demonstrate a strong modification with respect to the dipole radiation pattern in vacuum [21, 33]. For example, in a photonic crystal with incomplete bandgap, the angular-resolved emission rate is suppressed in the direction of the spatial stopband and strongly enhanced in the direction of the group velocity, which is stationary with respect to a small variation of the wave vector (photon focusing) [33]. Such an enhancement is the result of the bunching of many Bloch eigenwaves with different wave vectors in the same spatial direction due to the crystal anisotropy [34, 35]. For a coherent light source, this inevitably leads to the interference of the Bloch eigenwaves at the detector plane and additional modification of the spatial distribution of the emission intensity.

In this paper, the physical picture of the interference fringes formation in the far-field emission pattern of the two-level atom placed in a periodic medium is considered. The paper is organized as follows. The evaluation of the asymptotic form of the emitted intensity (7) is given in section II in the radiation zone. The physical explanation and the relevance of results for experimental observation are discussed in section III. In section IV a numerical example is given for a two-dimensional polymer photonic crystal. Section V summarized the main results of the paper.

II. ASYMPTOTIC FORM OF EMITTED INTENSITY

By taking into account the Bloch theorem, $\mathbf{A}_{n\mathbf{k}}(\mathbf{r}) = \mathbf{a}_{n\mathbf{k}}(\mathbf{r})e^{i\mathbf{k}_n\cdot\mathbf{r}}$, where $\mathbf{a}_{n\mathbf{k}}(\mathbf{r})$ is a lattice periodic function, and changing the k-space summation to the corresponding k-space integral, $\sum_{\mathbf{k}} \to \left(V/8\pi^3\right)\int d^3k$, Eq. (7) can be expressed as

$$I(\mathbf{r},\omega) = \left|\frac{\omega_0^2}{8\pi^3\varepsilon_0}\sum_n\int d^3\mathbf{k}_n\frac{(\mathbf{a}^*_{n\mathbf{k}}(\mathbf{r}_0)\cdot\mathbf{d})\,\mathbf{a}_{n\mathbf{k}}(\mathbf{r})}{\omega^2_{n\mathbf{k}}-(\omega_0+i\gamma)^2}e^{i\mathbf{k}_n\cdot(\mathbf{r}-\mathbf{r}_0)}\right|^2 \quad (8)$$

For large $|\mathbf{x}| = |\mathbf{r}-\mathbf{r_0}|$ the exponential function in the integral (8) oscillates rapidly. To evaluate the integral, the method of stationary phase can be used. As it was shown in [33], the principal contribution to the integral comes from the regions of the iso-frequency surface in the wave vector space, at which the eigenwave group velocity is parallel to observation direction $\mathbf{x}$. Then, the integral in Eq. (8) can be transformed to the form

$$I(\mathbf{r},\omega) \approx \left|\frac{\omega}{8\pi^2\varepsilon_0}\sum_\nu\sum_n\frac{(\mathbf{a}^{\nu *}_{n\mathbf{k}}(\mathbf{r}_0)\cdot\mathbf{d})\,\mathbf{a}^\nu_{n\mathbf{k}}(\mathbf{r})}{|\mathbf{V}^\nu_{n\mathbf{k}}|}\oint_{-\infty}^{\infty}d^2\mathbf{k}_n e^{i\mathbf{k}_n\cdot(\mathbf{r}-\mathbf{r}_0)}\right|^2, \quad (9)$$

where $\mathbf{V}^\nu_{n\mathbf{k}}$ is the group velocity of the Bloch eigenwave, the integration is over the iso-frequency surface $\omega_{n\mathbf{k}} = \omega_0$ and summation is taken over all stationary eigenwaves ν with a group velocity vector pointing in the observation direction $\mathbf{x} = \mathbf{r}-\mathbf{r_0}$.

The result of the integration in (9) depends on the local topology of iso-frequency surface $\omega_{n\mathbf{k}} = \omega_0$. It is convenient to introduce the local curvilinear coordinates ξ_i with the origin at the iso-frequency surface and with one of the coordinate aligned perpendicular to it, e.g., ξ_3. Then, a function $h(\xi_1,\xi_2) = \mathbf{k}_n\cdot\widehat{\mathbf{x}}$ can be expanded in a series near the wave vector of the eigenwave $(\nu,n,\mathbf{k})$:

$$h(\xi_1,\xi_2) = \mathbf{k}^\nu_n\cdot\widehat{\mathbf{x}} + \frac{1}{2}\sum_{i,j=1}^{2}\alpha^\nu_{ij}\xi_i\xi_j + \frac{1}{6}\sum_{i,j,k=1}^{2}\beta^\nu_{ijk}\xi_i\xi_j\xi_k + O(\xi_1,\xi_2)^4, \quad (10)$$

where

$$\alpha_{ij}^{\nu}=\left(\frac{\partial^2 h}{\partial\xi_i\partial\xi_j}\right)_{\nu},\qquad \beta_{ijk}^{\nu}=\left(\frac{\partial^3 h}{\partial\xi_i\partial\xi_j\partial\xi_k}\right)_{\nu}$$

and $\widehat{\mathbf{x}}$ is a unit vector in the observation direction $\mathbf{x}=\mathbf{r}-\mathbf{r_0}$. If the iso-frequency surface has a non-vanishing Gaussian curvature in the vicinity of the wave vector $\mathbf{k}_n^{\nu}$, only quadratic terms in the expansion (10) can be kept, leading to the following asymptotic from of the far-field intensity(9) [33]

$$I(\mathbf{r},\omega)\approx\left|\frac{\omega_0^2}{4\pi\varepsilon_0}\sum_{\nu}\sum_{n}\exp\left(-i\frac{\pi}{4}\left(\mathrm{sign}(\alpha_1^{\nu})+\mathrm{sign}(\alpha_2^{\nu})\right)\right)\frac{\left(\mathbf{A}_{n\mathbf{k}}^{\nu *}(\mathbf{r}_0)\cdot\mathbf{d}\right)\mathbf{A}_{n\mathbf{k}}^{\nu}(\mathbf{r})}{|\mathbf{V}_{n\mathbf{k}}^{\nu}|}\frac{1}{|K_{n\mathbf{k}}^{\nu}|^{1/2}|\mathbf{r}-\mathbf{r}_0|}\right|^2 \tag{11}$$

where $K_{n\mathbf{k}}^{\nu}=\alpha_{11}^{\nu}\alpha_{22}^{\nu}$ determines the Gaussian curvature of the iso-frequency surface at the point $\mathbf{k}_n=\mathbf{k}_n^{\nu}$ (stationary point) and summation is over all stationary points with $\mathbf{x}\cdot\mathbf{V}_{n\mathbf{k}}^{\nu}>0$.

The emission intensity far from an atom is proportional to the inverse Gaussian curvature of the iso-frequency surface, $\sim|K_{n\mathbf{k}}^{\nu}|^{-1}$, and to the inverse square of the distance between the source and the observation point, $\sim|\mathbf{x}|^{-2}$. The asymptotic energy flux shows the necessary amount of decrease with distance ($\sim|\mathbf{x}|^{-2}$), providing a finite value of the energy flux in any finite interval of a solid angle, that is, assuming non-vanishing Gaussian curvature. A vanishing curvature formally implies an infinite flux along the corresponding observation direction, leading to the photon focusing phenomenon [33, 36, 37].

Strictly speaking, the asymptotic behavior of the emission intensity (11) is valid only if quadratic terms in the expansion (10) do not vanish, so that all higher order terms in the expansion can be neglected. A parabolic point of the iso-frequency surface is an example of vanishing quadratic terms in (10). Generally, the Gaussian curvature is zero at a parabolic point and one (both) of the principal curvatures of the iso-frequency surface is zero. Actually, at parabolic points the asymptotic behavior of the emitted intensity, i.e., the dependence of the intensity on the inverse distance ($\sim|\mathbf{x}|^{-1}$) changes to the power of the inverse distance.

As an illustration one can consider the simple parabolic point $\mathbf{k}_0=\mathbf{k}_n^0$ in the vicinity of which the function $h(\xi_1,\xi_2)$ has the expansion [38]:

$$h(\xi_1,\xi_2)=\mathbf{k}_0\cdot\widehat{\mathbf{x}}_0+\frac{1}{2}\alpha\xi_1^2+\frac{1}{6}\beta\xi_2^3,\ \alpha=\alpha_{11}^0,\ \beta=\beta_{111}^0, \tag{12}$$

where $\widehat{\mathbf{x}}_0$ is the unit vector in the direction normal to the iso-frequency surface at the parabolic point $\mathbf{k}_0$. The local curvilinear coordinates ξ_i has the origin at the parabolic point $\mathbf{k}_0$, with the coordinates ξ_1 and ξ_2 aligned along the directions of the principal curvatures of the iso-frequency surface at this point and with the coordinate ξ_3 aligned along $\widehat{\mathbf{x}}_0$. For the parabolic point $\mathbf{k}_0$ (12) one of the principal curvature vanishes ($\alpha_{22}^0=0$), while another principal curvature remain non-zero. Using the expansion (12) the asymptotic form of the intensity (9) is given by:

$$I(\mathbf{r},\omega)\approx\left|\frac{\omega_0}{8\pi^2\varepsilon_0}\frac{\left(\mathbf{a}_0^{*}(\mathbf{r}_0)\cdot\mathbf{d}\right)\mathbf{a}_0(\mathbf{r})}{|\mathbf{V}_0|}e^{i\mathbf{k}_0\cdot\mathbf{x}}\oint_{-\infty}^{\infty}d\xi_1 d\xi_2\exp\left(i|\mathbf{x}|\left(\frac{\alpha}{2}\xi_1^2+\frac{\beta}{6}\xi_2^3\right)\right)\right|^2 \tag{13}$$

where $\mathbf{A}_0(\mathbf{r})=\mathbf{a}_0(\mathbf{r})e^{i\mathbf{k}_0\cdot\mathbf{r}}$ and $\mathbf{V}_0$ are the Bloch mode and the group velocity associated with the parabolic point $\mathbf{k}_0$, respectively. Calculating integrals in (13), leads to

$$\int_{-\infty}^{\infty}d\xi\exp\left(i\frac{x\alpha}{2}\xi^2\right)=\sqrt{\frac{2\pi}{x|\alpha|}}\exp\left(-\frac{i\pi}{4}\mathrm{sing}(\alpha)\right) \tag{14}$$

for the direction ξ_1 and

$$\int_{-\infty}^{\infty}d\xi\exp\left(i\frac{x\beta}{6}\xi^3\right)=\frac{3}{\sqrt[3]{x|\beta|}}\Gamma\left(\frac{4}{3}\right), \tag{15}$$

for direction ξ_2. Here $\Gamma\left(\frac{4}{3}\right)$ is the Gamma function. Now, combining (14) and (15) the following expression for the asymptotic vector potential associated with the parabolic point (12) can be obtained [39, 40]:

$$I(\mathbf{r},\omega)\approx\left|\frac{3}{2^{5/2}}\frac{\omega_0}{\pi^{3/2}\varepsilon_0}\exp\left(\frac{\pi}{4}(\mathrm{sign}(\alpha))\right)\Gamma\left(\frac{4}{3}\right)\frac{\left(\mathbf{A}_0^{*}(\mathbf{r}_0)\cdot\mathbf{d}\right)\mathbf{A}_0(\mathbf{r})}{|\mathbf{V}_0|}\frac{1}{|\alpha|^{1/2}|\beta|^{1/3}|\mathbf{r}-\mathbf{r}_0|^{5/6}}\right|^2. \tag{16}$$

The emission intensity associated with a parabolic point falls off with the distance as $|\mathbf{x}|^{-5/3}$ in contrast to the usual inverse square law $|\mathbf{x}|^{-2}$ for other directions.

If there are no additional singularities on the parabolic line, the product $|\alpha|\,|\beta|^{1/2} \sim K$, where K is the Gaussian curvature at an arbitrary point of the iso-frequency surface. Then the emission intensity is proportional to $K^{-1}\,|\beta|^{-1/6}$. Thus, at large $|\mathbf{x}|$, the energy flux along the direction corresponding to a parabolic point on the iso-frequency surface exceeds the energy flux along the direction corresponding to an elliptical point in the ratio $|\mathbf{x}|^{1/3}\,|\beta|^{1/6}$.

The expression (16) gives the asymptotic emitted intensity in the direction $\widehat{\mathbf{x}}_0$ associated with a parabolic point on the iso-frequency surface $\mathbf{k}_0$, so in the direction of the group velocity at the parabolic point. Now, the asymptotic intensity for directions $\widehat{\mathbf{x}}$ near the direction of that group velocity will be calculated. As before, the origin of the coordinates ξ_i is chosen at the parabolic point, where the direction of observation $\widehat{\mathbf{x}}$ is coincides with direction $\widehat{\mathbf{x}}_0$. It is assumed, that the principal curvature vanishes in the ξ_2 direction. Let the position $\mathbf{x}$ ($\mathbf{x}\|\widehat{\mathbf{x}}$) be described by coordinates x_i. Then, since $\mathbf{x}$ is nearly parallel to $\widehat{\mathbf{x}}_0$ one have from (12) [38]:

$$\xi_3 = \frac{1}{2}\alpha\xi_1^2 + \frac{1}{6}\beta\xi_2^3$$

and

$$\mathbf{k}_n \cdot \mathbf{x} \approx \mathbf{k}_0 \cdot \mathbf{x} + \xi_1 x_1 + \xi_2 x_2 + \left(\frac{1}{2}\alpha\xi_1^2 + \frac{1}{6}\beta\xi_2^3\right) x_3. \quad (17)$$

Using expansion (17) the asymptotic form of the intensity (9) is given by

$$I(\mathbf{r},\omega) \approx \left| \frac{\omega_0}{8\pi^2\varepsilon_0} \frac{(\mathbf{a}_0^*(\mathbf{r}_0)\cdot\mathbf{d})\,\mathbf{a}_0(\mathbf{r})}{|\mathbf{V}_0|} e^{i\mathbf{k}_0\cdot\mathbf{x}} \int_{-\infty}^{\infty} d\xi_1 e^{i\left(x_1\xi_1 + \frac{1}{2}\alpha|\mathbf{x}|\xi_1^2\right)} \int_{-\infty}^{\infty} d\xi_2 e^{i\left(x_2\xi_2 + \frac{1}{6}\beta|\mathbf{x}|\xi_2^3\right)} \right|^2 \quad (18)$$

where the fact that $|\mathbf{x}|$ and x_3 are approximately equal was used. The integral in (18) over ξ_1 is calculated simply to be

$$\int_{-\infty}^{\infty} d\xi_1 e^{i\left(x_1\xi_1 + \frac{1}{2}\alpha|\mathbf{x}|\xi_1^2\right)} = \frac{\sqrt{2\pi}}{|\alpha|^{1/2}\,|\mathbf{x}|^{1/2}} e^{-i\frac{x_1^2}{2\alpha|\mathbf{x}|}} e^{-\frac{i\pi}{4}\mathrm{sign}(\alpha)},$$

while the integral over ξ_2 results in

$$\int_{-\infty}^{\infty} d\xi_2 e^{i\left(x_2\xi_2 + \frac{1}{6}\beta|\mathbf{x}|\xi_2^3\right)} = \frac{2^{4/3}\pi}{|\beta|^{1/3}\,|\mathbf{x}|^{1/3}} \mathrm{Ai}\left(x_2 \frac{2^{1/3}}{|\beta|^{1/3}\,|\mathbf{x}|^{1/3}}\right),$$

where Ai is the Airy function. Then the asymptotic emitted intensity (18) is finally given by

$$I(\mathbf{r},\omega) \approx \left| \frac{1}{2^{7/6}} \frac{\omega_0}{\pi\varepsilon_0} \exp\left(-i\left(\frac{x_1^2}{2\alpha\,|\mathbf{x}|} + \frac{\pi}{4}\mathrm{sign}\,(\alpha)\right)\right) \frac{(\mathbf{A}_0^*(\mathbf{r}_0)\cdot\mathbf{d})\,\mathbf{A}_0(\mathbf{r})}{|\mathbf{V}_0|} \frac{1}{|\alpha|^{1/2}\,|\beta|^{1/3}\,|\mathbf{r}-\mathbf{r}_0|^{5/6}} \mathrm{Ai}\left(\frac{x_2}{a}\right) \right|^2, \quad (19)$$

where $a = (|\beta|\,|\mathbf{x}|\,/2)^{1/3}$.

As in the case of the asymptotic intensity (16), energy flux in the direction $\mathbf{x}$ falls off as $|\mathbf{x}|^{-5/3}$ and exceeds the energy flux along the other directions in the ratio $|\mathbf{x}|^{1/3}\,|\beta|^{1/6}$. The dependence of the energy flux in the plane of the vanishing principal curvature is given by the square of the Airy function $[\mathrm{Ai}\,(x_2/a)]^2$. When x_2/a is positive, the energy flux is small and exponentially drops while the angle between direction of observation and direction corresponded to the parabolic point increases (Fig. 1). For negative x_2/a, the flux oscillates rapidly and has a mean value averaged over one cycle proportional to $\sim (x_2/a)^{-1/2}$ (Fig.1). A mean value of the energy flux is then proportional to $|\alpha|^{-1}\,|\beta|^{-1/2} \sim K^{-1}$ and $|\mathbf{x}|^{-2}$ and coincides with the asymptotic energy flux associated with an elliptical point of iso-frequency surface (11), demonstrating focusing of the energy flux in the direction corresponding to the parabolic point of the iso-frequency surface.

III. INTERFERENCE OF BLOCH EIGENWAVES

The vanishing curvature of the iso-frequency surface results in the folds of the wave front (wave surface) [33]. Then, for the direction near the fold of the wave surface the field is a superposition of several Bloch eigenwaves (Fig. 2). In the far-field, where the source-to-detector distance is much larger than the source size and the wave-

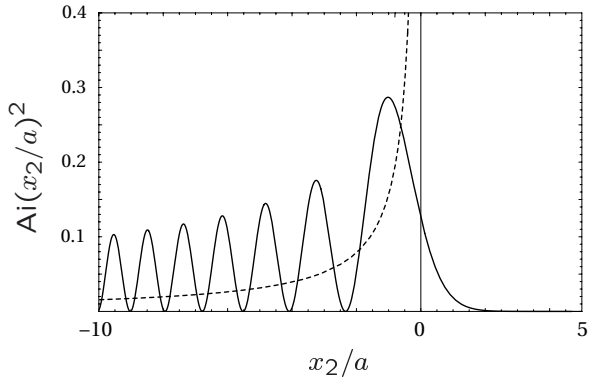

Figure 1: Plot of Airy function $[\mathrm{Ai}\,(x_2/a)]^2$ (solid line) and its mean value $(1/4\pi)^{-1}\,(x_2/a)^{-1/2}$ (dashed line). The dashed line can be considered as the "geometrical optics" approximation of the Airy function.

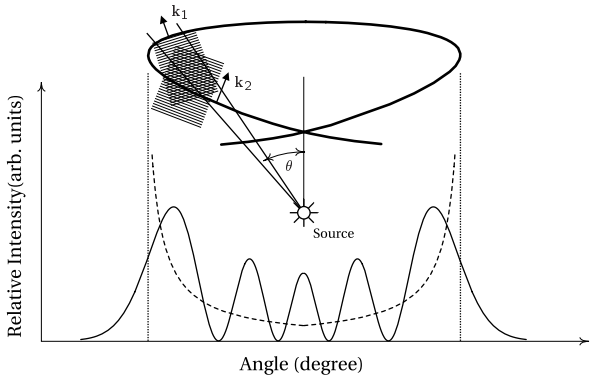

Figure 2: Diagram illustrating the self-interference of the Bloch eigenwaves in a photonic crystal. A section of the wave surface with a fold is presented (thick solid line). The asymptotic intensity (solid line) displays oscillations as the angle passes the fold section of the wave surface. The asymptotic intensity in the "geometrical optics" limit demonstrates focusing caustics in the direction of the folds (dashed line). Within a small solid angle the far-field of a point source consists on superposition of three Bloch eigenwaves with different wave vectors. These Bloch eigenwaves interfere leading to oscillations in the intensity distribution. Only two wave vectors are illustrated for clarity.

length, the part of the wave front limited to the small solid angle can be approximated as a Bloch eigenwave with the group velocity within this angle. If there is a relative difference in the lengths or directions of the wave vectors of Bloch eigenwaves, the eigenwaves can interfere yielding an oscillations in the energy flux distribution. This can be already seen from the general expression for the emitted intensity (7).

Two general conditions are required for the interference to occur. The polarization states of the Bloch eigenwaves must be nonorthogonal and the Bloch eigenwaves must overlap in space [41]. This kind of interference of the Bloch eigenwaves will be called further *a self-interference*, to stress that the field produced by the light source inside a photonic crystal can interfere with itself producing an interference patten in the energy flux distribution. A similar self-interference effect also happens in the case of ballistic phonons propagation in an acoustically anisotropic crystals [40, 42].

For a more qualitative measure of the self-interference effect the iso-frequency surface superimposed on a photonic crystal is considered in figure 3. Here evaluation presented by Hauser et al. [42] for the self-interference of ultrasound in a crystal is followed. In the figure 3, dots are parabolic points of zero curvature. The light source is located near the bottom surface of the photonic crystal and generates uniform distribution of wave vectors. The Bloch eigenwave with wave vector $\mathbf{k}_0$ propagates with the group velocity $\mathbf{V}_0$, normal to the iso-frequency surface at $\mathbf{k}_0$, arriving at the point $\mathbf{R}_0$ on the opposite surface of the crystal. Near the parabolic point the iso-frequency surface are practically flat, neighboring wave vectors have nearly the same group velocity. This gives rise to the high-intensity caustic in the detected intensity distribution (Fig. 3-left). If the detector is moved to a point $\mathbf{R}_1$ slightly away from $\mathbf{R}_0$, two distinct Bloch eigenwaves with different wave vectors $\mathbf{k}'_1$ and $\mathbf{k}'_2$ near $\mathbf{k}_0$ arrive at the detector (Fig. 3-right). If the surface were perfectly flat near $\mathbf{k}_0$, then $\mathbf{k}'_1 \cdot \mathbf{R}_1 = \mathbf{k}'_2 \cdot \mathbf{R}_1$, and the two eigenwaves would always remain in phase at the detector, interfering constructively. In reality the iso-frequency surface is curved near the parabolic point, so as $\mathbf{R}_1$ is rotated downward the corresponding waves begin to interfere destructively, producing an Airy pattern (Figs. 1-3). If $\mathbf{k}'_1$ and $\mathbf{k}'_2$ are close two $\mathbf{k}_0$, and that $\mathbf{q} \equiv \mathbf{k}'_1 - \mathbf{k}_0 \approx \mathbf{k}'_2 - \mathbf{k}_0$, then destructive interference will take place, if the total phase difference of the light as it travels through the sample, $2\mathbf{q} \cdot \mathbf{R}_1$, is an odd integer multiple of π.

Strictly speaking, there is one more Bloch eigenwave following in the observation direction in the fold region of the wave surface (Figs. 2-3). This eigenwave is depicted as $\mathbf{V}_1$ and $\mathbf{V}'_3$ in the left and right panels of figure 3, respectively. To obtain a complete picture of the self-interference near the fold of the wave surface, a three-wave interference should be taken into account, which would lead to more complicated interference patterns in the intensity distribution. Here, the influence of this third eigenwave is neglected for simplicity, hence this eigenwave usually has a relatively small group velocity and could arrive at the detector too late to interfere with the eigenwaves $\mathbf{k}'_1$ and $\mathbf{k}'_2$.

From the perspective of the self-interference effect, the mean value of the asymptotic energy flux (19) averaged over one cycle of Airy oscillations can be viewed as a "geometrical optics" approximation of the actual energy flux. This approximation then corresponds to the ray description of wave propagation, where the energy flux is simply proportional to the density of rays crossing a detector surface. In this picture the interference among different rays is neglected. Then, the emission rate enhancement in the focusing direction can also be inter-

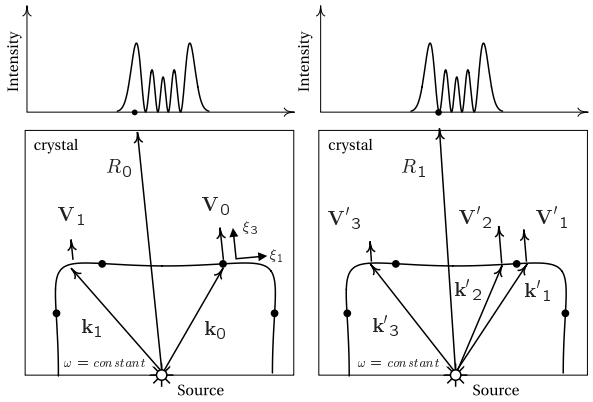

Figure 3: Schematic of self-interference in a photonic crystal. The iso-frequency surface is a sketch of the iso-frequency surface of a real 2D photonic crystal. The plot on the top is the detected intensity distribution. Left: For the wave vector $\mathbf{k}_0$, the group velocity is $\mathbf{V}_0$ and the wave arrives at $\mathbf{R}_0$. Right: There are two eigenwaves with different wave vectors $\mathbf{k}'_i$, which group velocity points in the same direction $\mathbf{R}_1$. The difference in the wave vectors of these eigenwaves results in the waves arriving at $\mathbf{R}_1$ with different phases and leads to interference.

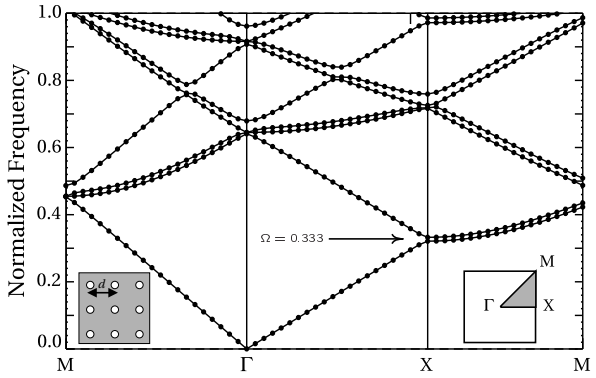

Figure 4: Photonic band structure of the square lattice of air holes made in a polymer. Polymer has the refractive index 1.56. Radius of holes is $r = 0.15d$, where d is the lattice period. The band structure is given for TM polarization. The frequency is normalized to $\Omega = \omega d/2\pi c = d/\lambda$. c is the speed of light in the vacuum. Insets show the first Brillouin zone (right) and a part of the lattice (left).

preted as the relative increase of the rays density or as an increased probability of the photon emission in this observation direction. As it has been mentioned above, the mean value of the asymptotic flux (19) coincides with the asymptotic energy flux (11) derived for elliptical points of the iso-frequency surface. So, the asymptotic energy flux (11) corresponded to an elliptical point can be also considered as a "geometrical optics" approximation, and can be used for all points of the iso-frequency surface within this approximation.

In a typical experiment the differences between the energy flux (19) and its "geometrical optics" approximation (11) will be reduced by the effect of the finite size of the light source and the detector. It is clear that if the linear dimensions of the source area and detector are L, the intensity is averaged over x_2 values with a spread of L. To see the oscillations of the energy flux one therefore needs $L \leq \Delta\theta \times R_1$, where R_1 is the distance between the source and the detector and $\Delta\theta$ is an angular separation of the fringes of intensity distribution.

To estimate this angular separation, Bloch eigenwaves $\mathbf{k}'_1$ and $\mathbf{k}'_2$ are further approximated by plane waves. Then their superposition at the detector position $\mathbf{R}_1$, assuming that they have the same polarization, is [42]:

$$e^{i\mathbf{k}'_1\cdot\mathbf{R}_1} + e^{i\mathbf{k}'_2\cdot\mathbf{R}_1} = 2\cos\left(\Delta\mathbf{k}\cdot\mathbf{R}_1\right)e^{i\mathbf{k}_0\cdot\mathbf{R}_1},$$

which is a plane wave with average wave vector $\mathbf{k}_0 = \left(\mathbf{k}'_1 + \mathbf{k}'_2\right)/2$, modulated by a cosine function with effective wave vector $\Delta\mathbf{k}/2 = \left(\mathbf{k}'_2 - \mathbf{k}'_1\right)/2$. When $\Delta\mathbf{k}\cdot\mathbf{R}_1 = \Delta k_\parallel R_1 = \pi$, the waves interfere destructively at the detector. To estimate $\Delta k_\parallel$ a local Cartesian coordinate system ξ_i with the origin at $\mathbf{k}_0$ and ξ_3 along $\mathbf{V}_0$ is chosen as it is shown in the figure 3-left. Then, the iso-frequency surface near the parabolic point can by parametrized as $\xi_3 = -a\xi_2^3/k_0$ and $\Delta k_\parallel = -2\xi_3 = 2a\xi_2^3/k_0^2$ [42]. Therefore, the first minimum in the intensity will occur when

$$\xi_2 = \left(\pi k_0^2/2aR_1\right)^{1/3} \sim R_1^{-1/3}\lambda^{-2/3},$$

where $\lambda = 2\pi/k_0$ is the average wavelength. Finally, the coordinate-space angle between the intensity maximum and the first minimum is given by [42]:

$$\Delta\theta \approx \left|\mathbf{V}'_1 - \mathbf{V}_0\right|/\mathbf{V}_0 = 3a\left(\pi/2ak_0R_1\right)^{2/3} \sim \left(\lambda/R_1\right)^{2/3}. \quad (20)$$

Then for optical wavelength, e.g., 500 nm, and a distance to the detector of 1 cm the linear dimension of the light source and the spatial resolution of the detector should be smaller than 10 μm. So, in most experiments the "geometrical optics" approximation (11) reasonably represents an asymptotic emission intensity of the light source inside a photonic crystal.

IV. NUMERICAL EXAMPLE

In this section different approximations of the light emission pattern, discussed in section II, are compared. Numerical calculations are done for a point source placed inside a two-dimensional polymer photonic crystal. A point source produces an isotropic and uniform distribution of wave vectors $\mathbf{k}_n$ with the frequency ω_0. Then, the asymptotic field in (9) and (11) should be averaged over the dipole moment orientation, which yields a factor of $|\mathbf{d}|/3$.

As it was pointed out in section II, the main contribution to the far-field of a point source inside a photonic crystal comes from the vicinity of the wave vector of the eigenmodes with the group velocity in the observation

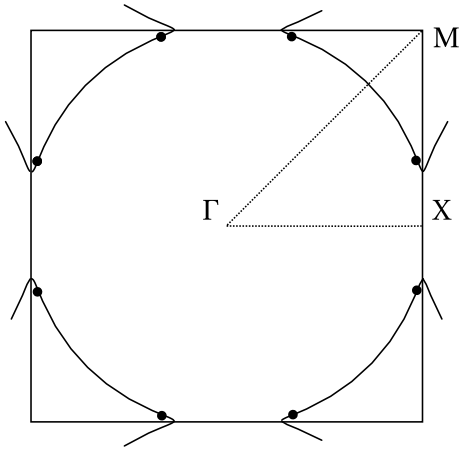

Figure 5: Iso-frequency contour of the square lattice photonic crystal (Fig. 4) for the normalized frequency $\Omega = 0.333$. Parabolic point are marked by the black dots. The first Brillouin zone of the lattice is plotted in order to show the spatial relation between zone boundary and iso-frequency contours.

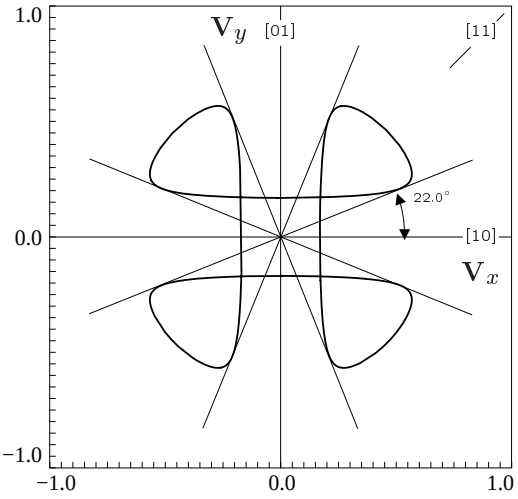

Figure 6: Wave contour corresponded to the normalized frequency $\Omega = 0.333$. The group velocity is plotted in the units of the speed of light in vacuum. The directions corresponded to the folds of the wave contour are shown.

direction. That means that the far-field emission intensity of a point source is mainly given by the square of the integral in (9)

$$I_w \sim \left| \oint_{-\infty}^{\infty} d^2\mathbf{k}_n e^{i\mathbf{k}_n(\mathbf{r}-\mathbf{r}_0)} \right|^2 . \tag{21}$$

In what follows, the contribution only from one photonic band is considered. In the "geometrical optics" approximation (11) the main contribution to the far-field emission intensity is then given by an inverse Gaussian curvature of the iso-frequency surface,

$$I_g \sim \sum_{\nu} |K^{\nu}_{n\mathbf{k}}| \, .^{-1} \tag{22}$$

The angular distribution of the far-field intensity depends on the topology of the iso-frequency surface of the crystal at the emission frequency (21-22). In what follows, an infinite two-dimensional square lattice of air holes in a polymer background is considered. Polymer has the refractive index $n = 1.56$, radius of holes is $r = 0.15d$, where d is the lattice period. The consideration is limited to the in-plane propagation of the TM mode of the crystal. The photonic band structure of such a photonic crystal is presented in the figure 4. The band structure has been calculated using the plane wave expansion method [43].

The iso-frequency contours for the normalized frequency $\Omega = 0.333$ is presented in figure 5. The frequency belongs to the first photonic band and it is within the first stopband in the ΓX direction of the crystal. To plot an iso-frequency contour, the photonic band structure for all wave vectors within the irreducible Brillouin zone was calculated and then an equation $\omega(\mathbf{k}) = \omega_0$ was solved for a given frequency ω_0. The iso-frequency contour is an *open* contour and has alternating regions of the Gaussian

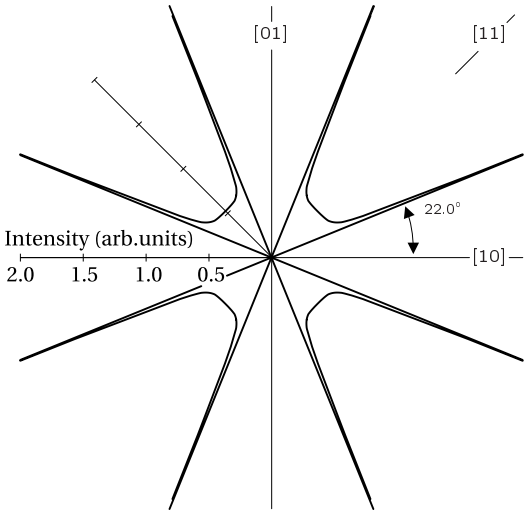

Figure 7: Angular distribution of radiative power corresponding to the normalized frequency $\Omega = 0.333$. The directions of infinite radiative power (caustic) coincide with the directions of the folds of the wave contour (Fig. 6).

curvature with a different sign. Parabolic points, where the Gaussian curvature vanishes, are marked by black dots in the figure 5. The vanishing curvature results in the folds of the wave contour and in the focusing of the light in the folds direction [33]. The wave contour corresponding to the iso-frequency $\Omega = 0.333$ is presented in the figure 6. A pair of the parabolic points in the first quarter of the Brillouin zone results in a cuspidal structure of the wave contours in the first quarter of the coordinate space. In the figure 7 the polar plot of the main contribution to the far-field intensity in the "geometrical optics" approximation (22) is presented. The energy flux is strongly anisotropic, showing relatively small intensity

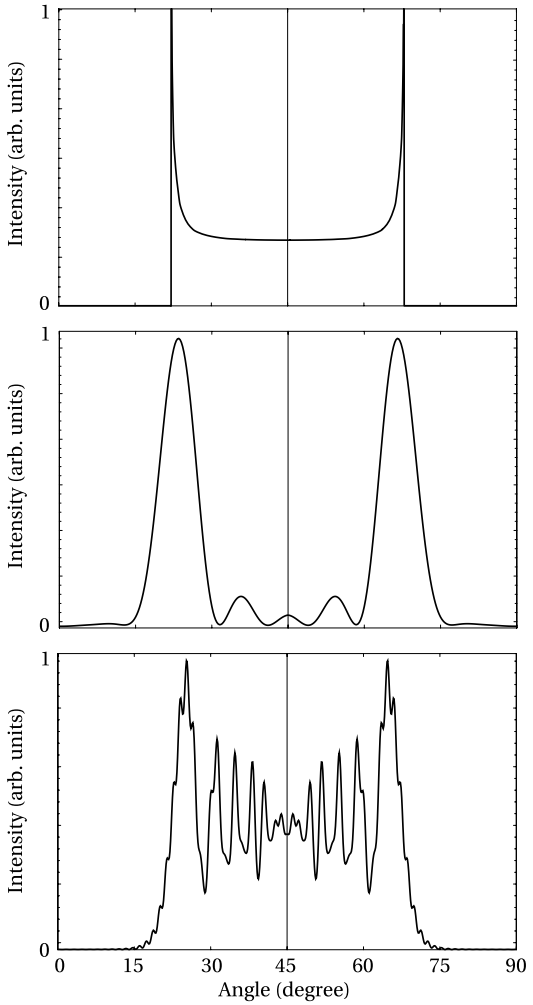

Figure 8: "Geometrical optics" (22) and "wave optics" (21) approximations of the far-field emission intensity. Normalized frequency is $\Omega = 0.333$. The distance between a point source and a detector is 100 lattice periods. The top panel is for the "geometrical optics" approximation. The middle and bottom panels are for the "wave optics" approximations. See text for more details.

in the directions of the stopband, and infinite intensity (caustics) in the directions of the folds.

In figure 8 the comparison of the "geometrical optics" (22) and "wave optics" (21) approximations of the far-field emission intensity is given. A normalized inverse Gaussian curvature of the iso-frequency surface $\Omega = 0.333$ is presented in the top panel. Focusing directions, 22° apart from the [10] direction of the square lattice, are clearly seen. The integral (21) evaluated for the distance 100 period apart from the point source is given in the middle and the bottom panels of figure 8. The normalized intensity distribution presented in the middle panel was calculated by reducing the integration limits in (21) to the close neighborhood of the parabolic point of the iso-frequency surface. Then the result of the integration is similar to one in (19) and an angular distribution of the emission intensity resembles the square of the Airy function. Actually, this approximation takes into account an interference of only two Bloch eigenwaves in the fold region. If the three wave interference is taken into account, by extending the integration limits in (21)

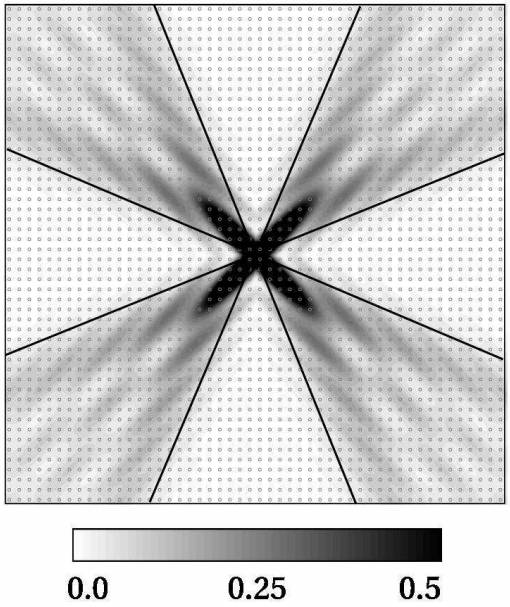

Figure 9: An asymptotic map of the intensity distribution inside a 50×50 photonic crystal. Normalized frequency is $\Omega = 0.333$. The structure of the crystal is superimposed on the field map. Folds directions are shown by black lines.

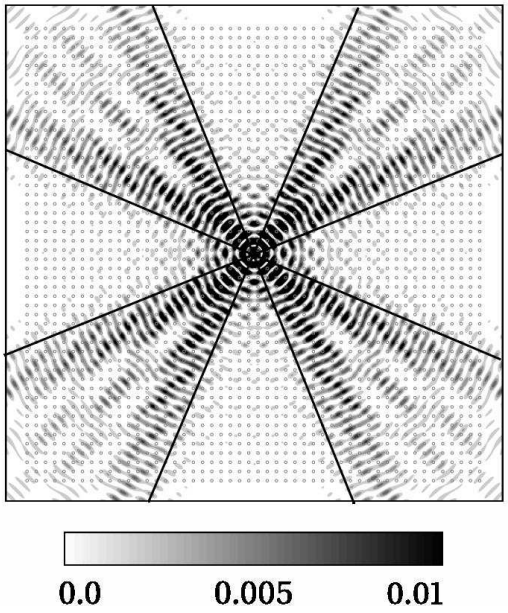

Figure 10: FDTD calculation. Map of the modulus of the Poynting vector field for a 50×50 rod photonic crystal excited by a point isotropic source with the normalized frequency $\Omega = 0.333$. The asymptotic directions of photon focusing caustics are shown as black lines.

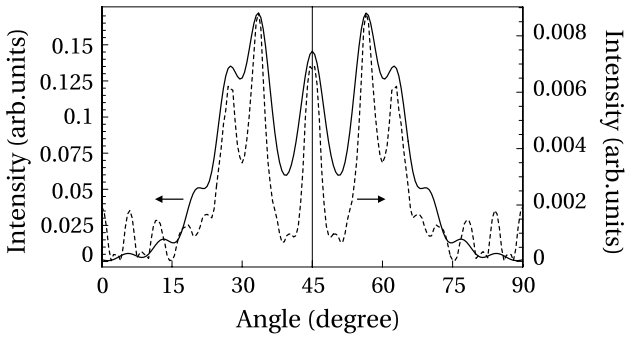

Figure 11: The comparison of the intensity distribution for the asymptotic (solid line) and the FDTD (dashed line) calculations. The distance between the point source and the detector is 20 lattice periods.

over all iso-frequency surface in the first quarter of the Brillouin zone, a more complex interference pattern appears in the angular emission intensity distribution (Fig. 8-bottom). Both "wave optics" approximations show an intensity enhancement along fold directions.

In figure 9 a two dimensional map of the intensity distribution inside a 50×50 photonic crystal is presented. The intensity distribution was calculated using Eq. (21) by integration over complete iso-frequency contour $\Omega = 0.333$. The structure of the crystal is superimposed on the field map. Folds directions are shown by black lines. The focusing of the light in the fold direction together with an Airy-like oscillations between folds directions are clearly seen in figure 9.

To substantiate an asymptotic analysis, the finite difference time domain (FDTD) calculations was done [44, 45]. The simulated structure was a 50×50 lattice. The crystal is surrounded by an extra $2d$ wide layer of polymer. The simulation domain was discretized into squares with a side $\Delta = d/32$. The total simulation region was 1728×1728 cells plus 8-cell wide perfectly matched layer (PML) [46]. The point isotropic light source was modeled by a current density source [44, 45] with a homogeneous spacial dependence and sinusoidal temporal dependence of the signal.

In figure 10 the map of the modulus of the Poynting vector field is shown, when the crystal is excited by a point isotropic source. The point source is placed in the middle of the crystal. A field map is shown for one instant time step. The snap-shots were captured after 10000 time steps, where the time step was 4.38×10^{-17} s (0.99 of the Courant value). The structure of the crystal is superimposed on the field map. One can see, that the emitted light is focused in the directions of the folds (black lines). Moreover, an interference pattern between the folds directions is in a reasonable agreement with the interference pattern predicted using the asymptotic analysis (Fig. 9). For the FDTD calculations, a periodic modulation of the intensity in the radial direction will go away if time averaging is performed. The comparison of the intensity distribution, 20 periods apart from the point source is given in figure 11. A reasonable agreement between interference minima and maxima positions for the asymptotic (solid line) and the FDTD (dashed line) calculations is shown. The disagreement in the absolute values of the angular intensity distributions is mainly because of the prefactor of the integral in (9) which was neglected in (21) for simplicity.

V. SUMMARY

It was shown, that the intensity modulation of the angular resolved emission spectra is not only due to the emission rate modification, but also is the result of the interference of several photonic crystal eigenmodes with different wave vectors approaching detector at the same moment of time. Using an asymptotic analysis of classical Green function, "geometrical optics" and "wave optics" approximations of the emitted intensity due to a two-level atom were introduced in the radiation zone. The physical reasons for the interference pattern formation and the possibilities of experimental observation of them were discussed. A numerical example was given in the case of polymer two-dimensional photonic crystal. It was shown that rigorous FDTD calculations are in a reasonable agreement with the developed approximate analysis.

Acknowledgments

This work was partially supported by the EU-IST project APPTech IST-2000-29321, the BMBF project PCOC 01 BK 253 and the DFG Research Unit 557.

[1] V. P. Bykov, Soviet Physics - JETP **35**, 269 (1972).
[2] E. Yablonovitch, Phys. Rev. Lett. **58**, 2059 (1987).
[3] S. John and J. Wang, Phys. Rev. Lett. **64**, 2418 (1990).
[4] J. P. Dowling and C. M. Bowden, Phys. Rev. A **46**, 612 (1992).
[5] T. Suzuki and P. K. L. Yu, J. Opt. Soc. Am. B **12**, 570 (1995).
[6] K. Sakoda and K. Ohtaka, Phys. Rev. B **54**, 5732 (1996).
[7] S. Nojima, Jpn. J. Appl. Phys. 2 **37**, L565 (1998).
[8] K. Busch, N. Vats, S. John, and B. C. Sanders, Phys. Rev. E **62**, 4251 (2000).
[9] Y. Xu, R. K. Lee, and A. Yariv, Phys. Rev. A **61**, 033807 (2000).
[10] Z. Y. Li, L. L. Lin, and Z. Q. Zhang, Phys. Rev. Lett. **84**, 4341 (2000).
[11] V. Lousse, J. P. Vigneron, X. Bouju, and J. M. Vigoureux, Phys. Rev. B **64**, 201104R (2001).
[12] C. Hermann and O. Hess, J. Opt. Soc. Am. B **19**, 3013

(2002).
[13] J. P. Dowling, M. Scalora, M. J. Bloemer, and C. M. Bowden, J. Appl. Phys. **75**, 1896 (1994).
[14] H. Hirayama, T. Hamano, and Y. Aoyagi, Appl. Phys. Lett **69**, 791 (1996).
[15] M. Boroditsky, R. Vrijen, T. F Krauss, R. Coccioli, R. Bhat, and E. Yablonovitch, IEEE J. Lightwave Technol. **17**, 2096 (1999).
[16] S. V. Gaponenko, V. N. Bogomolov, E. P. Petrov, A. M. Kapitonov, A. A. Eychmueller, A. L. Rogach, I. I. Kalosha, F. Gindele, and U. Woggon, J. Lightwave Technol. **17**, 2128 (1999).
[17] B. Temelkuran, M. Bayindir, E. Ozbay, R. Biswas, M. M. Sigalas, G. Tuttle, and K. M. Ho, J. Appl. Phys **87**, 603 (2002).
[18] H. P. Schriemer, H. M. van Driel, A. F. Koenderink, and W. L. Vos, Phys. Rev. A **63**, 011801R (2000).
[19] S. G. Romanov, T. Maka, C. M. Sotomayor Torres, M. Muller, and R. Zentel, Appl. Phys. Lett. **79**, 731 (2001).
[20] A. F. Koenderink, L Bechger, H. P. Schriemer, A. Lagendijk, and W. L. Vos, Phys. Rev. Lett. **88**, 143903 (2002).
[21] S. G. Romanov, D. N. Chigrin, V. G. Solovyev, T. Maka, N. Gaponik, A. Eychmuller, A. L. Rogach, and Sotomayor Torres, Phys. Stat. Sol. **197**, 662 (2003).
[22] A. F. Koenderink, L Bechger, A. Lagendijk, and W. L. Vos, Phys. Stat. Sol. **197**, 648 (2003).
[23] K. Sakoda, Opt. Express **4**, 167 (1999).
[24] J. D. Joannopoulos, R. D. Meade, and J. N. Winn, *Photonic crystals: molding the flow of light* (Princeton University Press, Princeton NJ, 1995).
[25] R. Coccioloi, M. Boroditsky, K. W. Kim, Y. Rahmat-Samii, and E. Yablonovitch, Inst. Elct. Eng. Pros.–Optoelectron. **145**, 391 (1998).
[26] O. J. Painter, A. Husain, A. Scherer, J. D. O'Brien, I. Kim, and P. D. Dapkus, J. Lightwave Tech. **17**, 2081 (1999).
[27] E. M. Purcell, Phys. Rev. **69**, 681 (1946).
[28] H. T. Dung, L. Knöll, and D.-G. Welsch, Phys. Rev. A **62**, 053804 (2000).
[29] R. Sprik, B. A. Van Tiggelen, and A. Lagendijk, Europhys. Lett. **35**, 265 (1996).
[30] R. C. McPhedran, L. C. Botten, J. McOrist, A. A. Asatryan, C. M. de Sterke, and N. A. Nicorovici, Phys. Rev. E **69**, 016609 (2004).
[31] K. Sakoda, *Optical Properties of Photonic Crystals* (Springer, Berlin, 2001).
[32] R. J. Glauber and M. Lewenstein, Phys. Rev. A **43**, 467 (1991).
[33] D. N. Chigrin, Phys. Rev. E **70**, 056611 (2004).
[34] R. Zengerle, J. Mod. Optics **34**, 1589 (1987).
[35] P. St. J. Russell, Appl. Phys. B: Photophysics & Laser Chemistry **B39**, 231 (1986).
[36] P. Etchegoin and R. T. Phillips, Phys. Rev. B **53**, 12674 (1996).
[37] D. N. Chigrin and C. M. Sotomayor Torres, Optics and Spectroscopy **91**, 484 (2001).
[38] A. M. Kossevich, *The Crystal Lattice* (Wiley, Berlin, 1999).
[39] A. A. Maradudin, in *Phonons and Phonon Interactions*, edited by T. A. Bak (Benjamin, New York, 1964), pp. 424–504.
[40] H. J. Maris, Phys. Rev. B **28**, 7033 (1983).
[41] P. St. J. Russell, Phys. Rev. A **33**, 3232 (1986).
[42] M. R. Hauser, R. L. Weaver, and J. P. Wolfe, Phys. Rev. A **33**, 3232 (1986).
[43] S. G. Johnson and J. D. Joannopoulos, Opt. Express **8**, 173 (2001).
[44] A. Taflove, *Computational Electrodynamics: The Finite-Difference Time-Domain Method* (Artech House, Norwood, 1995).
[45] D. M. Sullivan, *Electromagnetic Simulation Using the FDTD Method* (IEEE Press, New York, 2002).
[46] J. P. Berenger, J. Comp. Phys. **114**, 185 (1994).